Progress In Electromagnetics Research M, Vol. 52, 79–87, 2016

EMI Shielding Effectiveness of Composites Based on Barium Ferrite, PANI, and MWCNT

Muhammad H. Zahari[1], Beh H. Guan[1, *], Cheng E. Meng[2], Muhammad F. C. Mansor[3], and Lee K. Chuan[1]

Abstract—An electromagnetic interference (EMI) shielding material based on the composite of $BaFe_{12}O_{19}$, polyaniline (PANI) and multi-walled carbon nanotube (MWCNT) was proposed. The constituents of the composite were brought together through mechanical mixing and the *in-situ* polymerization of aniline on the $BaFe_{12}O_{19}$ and MWCNT surfaces. A series of composite with different MWCNT wt% loadings (0, 5, 10, 15, 20 and 25wt%) was prepared, and its effect on the EMI shielding performance was investigated. X-ray diffraction analysis was performed on all synthesized composites to confirm the phase formations. FESEM micrographs reveal the PANI particle formation on both $BaFe_{12}O_{19}$ and MWCNT surfaces. Electromagnetic measurements were done by using a rectangular waveguide connected to a network analyser to obtain the permeability, μ_r, permittivity, ε_r, and shielding effectiveness (SE_A and SE_R). The increase in the MWCNT loading results in the enhancement of the composite's shielding performance to a certain limit. Optimum EMI shielding performance is shown by sample PBM4 (20wt% MWCNT) with SE_R and SE_A values of 5.14 dB at 8.2 GHz and 36.41 dB at 12.4 GHz, respectively. The influence of different MWCNT loadings (0, 5, 10, 15, 20 and 25wt%) on the EMI shielding performance of a composite consisting of $BaFe_{12}O_{19}$, polyaniline (PANI) and multi-walled carbon nanotube (MWCNT) were investigated.

1. INTRODUCTION

Electromagnetic interference (EMI) is a type of modern day pollution which has become a major concern especially with the rapid development of communication technology. The phenomenon, whose initial concerns were only among military technology, has become very prominent to the public as more digital devices are made available to the mass consumer market [1]. Due to the higher number of electronic devices existing in close proximity to each other, there is a higher chance for the electronic components to be susceptible to unwanted electromagnetic emissions. The effects of these unwanted emissions can be noises interfering with signal transmissions to total data loss and device failure. It is thus important to introduce a shielding mechanism that is able to limit unwanted emission towards susceptible devices as well as to limit any potential interference that may originate from the device itself. Depending on the desired practical application, there is a very wide variety of shielding materials that are able to be utilized. For example, hexagonal ferrites have long been known to possess salient properties such as good chemical stability [2], large crystal anisotropy [3, 4], and big values of permeability [5, 6], enabling it to exhibit good electromagnetic wave absorbing properties. The discovery of its high electrical conductivity have renewed interests in the intrinsically conducting polymer (ICP), polyaniline (PANI), and its possible applications for microwave absorption [7–9]. Carbon based shielding materials have seen widespread adoption in various fields of application due to their light weight and are known to

Received 7 August 2016, Accepted 4 November 2016, Scheduled 21 November 2016

* Corresponding author: Beh Hoe Guan (beh.hoeguan@petronas.com.my).

[1] Fundamental and Applied Sciences Department, Universiti Teknologi Petronas, 32610, Seri Iskandar, Perak Darul Ridzuan, Malaysia. [2] School of Mechatronic Engineering, Universiti Malaysia Perlis (UniMAP), 02600 Arau, Perlis, Malaysia. [3] School of Material Engineering, Universiti Malaysia Perlis (UniMAP), 02600 Arau, Perlis, Malaysia.

show good electrical properties [10]. Among the allotropes of carbon, MWCNT has shown promising EMI shielding capabilities through synergistic effects when being paired with other types of shielding materials [11, 12].

All these materials have individually shown potential for electromagnetic shielding applications. However, their practical application is severely limited due to several impeding factors. Ferrites, while having shown considerable magnetic loss and absorbing capabilities, are limited to static and permanent applications due their high density and difficulty in forming them into complex structures [13]. The application of ICPs is hindered by their poor magnetic loss and narrow absorption bandwidth [14] while carbon-based shielding materials suffer from relatively complex and costly fabrication process [15]. To overcome the aforementioned problems, researchers have since developed hybrid materials that combine several shielding materials to offset respective limitation of the materials while still retaining its enhanced shielding properties. Various combinations of materials with optimum shielding capabilities have since been developed [7, 9, 16–18].

In this research work, a ternary composite shielding material based on the M-type hexagonal ferrite, $BaFe_{12}O_{19}$, intrinsically conducting polymer, polyaniline (PANI) and multi-walled carbon nanotubes (MWCNT) is prepared through *in-situ* polymerization. The effect of the MWCNT addition in each synthesized composite on the composite material's shielding capability is determined through electromagnetic measurements.

2. METHODS

The main constituents of the composite were brought together through mechanical mixing and the subsequent polymerization of aniline. The multi-walled carbon nanotubes (MWCNT) were readily obtained from a reputable supplier (Sigma-Aldrich). The ferrite component of the composite was synthesized through the wet gel combustion method as described in the following subsection.

2.1. Ferrite Synthesis

Stoichiometric amounts of the nitrate salts of barium, ($Ba(NO_3)_2$), and iron, ($Fe(NO_3)_3.9H_2O$), were used in this synthesis with citric acid as the chelating agent (Citric acid to metal ion ratio, 2 : 1). The precursors were mixed together and the pH of the mixture was brought up to 7 by using ammonia solution. The dark green mixture was allowed to stir overnight with heating until it thickened into a gel. The gel was then directly combusted in a box furnace at 300°C for 10–20 minutes to produce a raised, porous compound. The compound was calcined to 950°C to obtain the desired ferrite phase with the chemical formula, $BaFe_{12}O_{19}$, and was ready to be used in the composite synthesis.

2.2. Composite Synthesis

The ratio among barium ferrite, aniline and MWCNT was taken as $(50 - x/2)BaFe_{12}O_{19}$:$(50 - x/2)$Aniline:$(x)$MWCNT, where x represents the wt% of MWCNT addition with respect to the final composite. Ammonium persulfate (APS), in the ratio of 1.05 : 1 to aniline, was used as the oxidant. Table 1 lists the synthesized composites with the respective MWCNT loadings.

Table 1. Synthesized composites.

Sample label	MWCNT wt%, $x =$
PBM0	0
PBM1	5
PBM2	10
PBM3	15
PBM4	20
PBM5	25

Suitable amounts of $BaFe_{12}O_{19}$ and MWCNT were dispersed in 50 ml distilled water, which was mechanically stirred for 30 minutes in an ice bath. Simultaneously, aniline, in 0.1 M of HCl, and APS, in 50 ml of distilled water, were cooled to $\pm 3^{\circ}$C in a separate ice bath. The aniline mixture was then added to the ferrite-CNT mixture and allowed to stir further for 30 minutes. The polymerization process was initiated by the drop-wise addition of the APS solution to the mixture. The mixture was left to stir and reacted completely for 6 hours, while still maintaining the temperature at $\pm 3^{\circ}$C. The dark greenish-brown compound obtained was filtered and repeatedly washed with distilled water and ethanol until the filtrate became colorless. It was dried in a drying oven at 80°C overnight. The composite synthesis was then complete and ready for characterization.

2.3. Characterization

Structural analysis was performed through x-ray diffraction (XRD) analysis by using an x-ray diffractometer (Bruker: D8 Advance XRD). The morphological aspects of the synthesized samples were observed through the micrographs taken by an FESEM LEO 1525, field-emission scanning electron microscope (FESEM). The room-temperature conductivity was measured by using a 4-point resistivity measurement system. For electromagnetic measurement purposes, the composite was mixed paraffin wax in the wt% ratio of 70 : 30 and was pressed into rectangular solids with the dimensions, 22.86 mm × 10.16 mm × 4.5 mm. Electromagnetic parameters were measured by utilizing an Agilent Technologies E8362B PNA Network Analyzer at the frequency range 8.2–12.4 GHz. The setup is as shown in Figure 1.

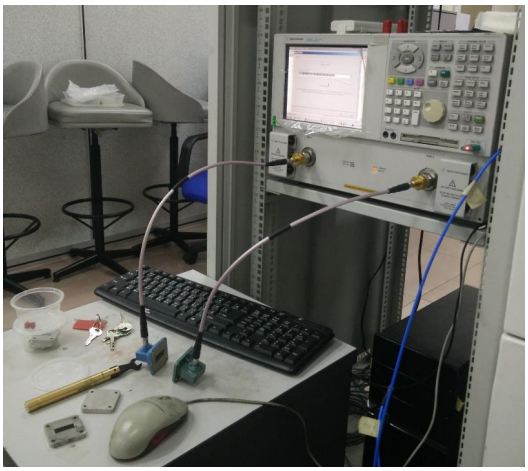

Figure 1. Electromagnetic measurement setup.

3. RESULTS AND DISCUSSION

3.1. Structural Characterization

Figure 2 shows the XRD patterns of the prepared composite samples with different MWCNT loadings. It can be easily discerned that the composite synthesis process does not result in any structural change towards the magnetoplumbite structure of $BaFe_{12}O_{19}$ as the main characteristic peaks of the ferrite material is still evident albeit with a decrease in its intensity. The main characteristic peaks of the synthesized composite with the hkl indexes of (110), (017), (114), (023), (025), (026), (0 2 11) and (220), present at $2\theta = 30.35^{\circ}$, 32.17°, 34.14°, 37.11°, 40.31°, 42.45°, 56.50° and 63.11°, respectively, matches well to that of the $BaFe_{12}O_{19}$ standard sample (ICSD98-010-6617).

It is apparent that the increased presence of MWCNT would indirectly lead to the decreased intensity of the main peaks attribute to the $BaFe_{12}O_{19}$. Sample PBM0 retained the intensity of the prominent peaks of the ferrite while a significant decrease in the intensity of the same characteristic

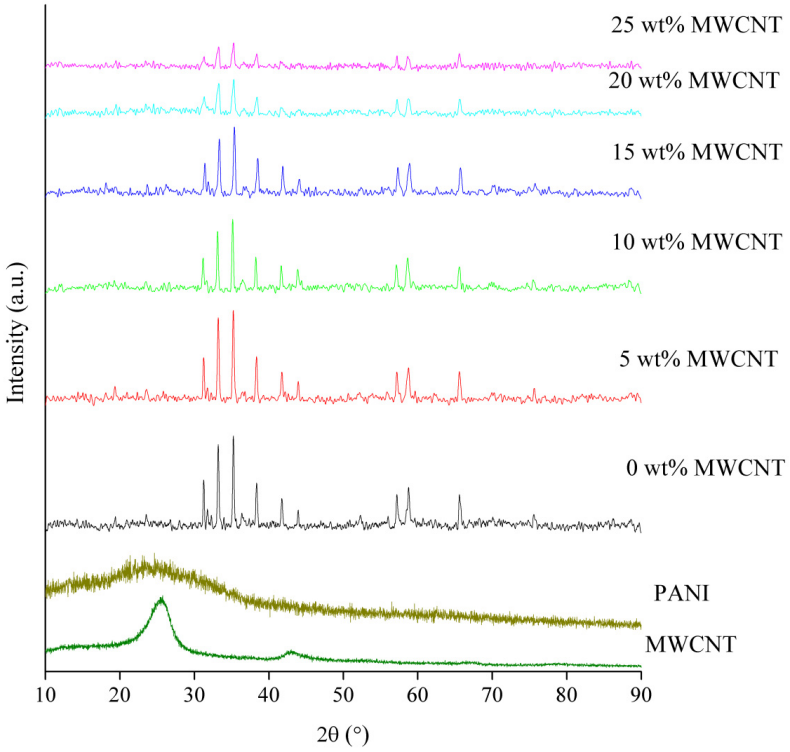

Figure 2. XRD analysis of composite synthesized with different MWCNT loadings and of pure PANI and MWCNT.

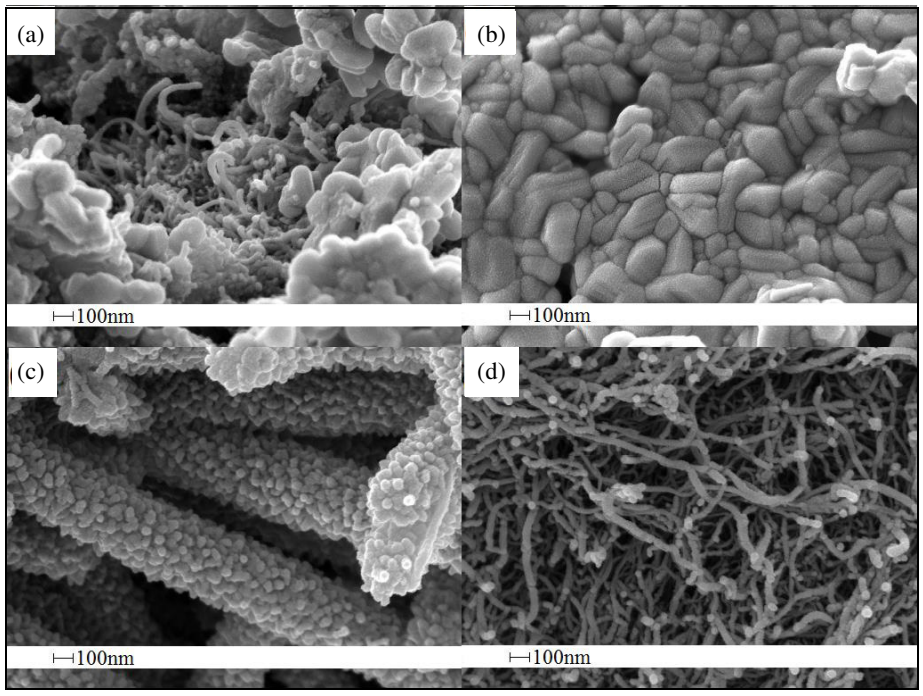

Figure 3. Micrographs of samples: (a) PBM4, (b) $BaFe_{12}O_{19}$, (c) polyaniline and (d) MWCNT taken at 50 k magnification.

peaks was seen as the MWCNT loading reaches 25wt% (PBM5). The decreasing amount of ferrite compound within the composite led to the peak intensity reduction.

Micrographs of the sample were taken through FESEM to investigate the surface morphology of the synthesized samples. Figure 3(a) shows the micrograph of sample PBM4 alongside that of $BaFe_{12}O_{19}$ (Figure 3(b)), PANI (Figure 3(c)), and MWCNT (Figure 3(d)). Due to the nature of the ferrite synthesis method used, $BaFe_{12}O_{19}$ particles observed in both Figures 3(a) and 3(b) are in agglomerated form with particle sizes ranging between 60.52 nm and 457.60 nm [19]. The PANI particles are seen to form on both $BaFe_{12}O_{19}$ and MWCNT surfaces. This is in contrast with the tubular structure normally associated with pure PANI when the polymerization process does not involve contact with foreign particles as shown by the structure in Figure 3(c).

3.2. Electrical Property

The conductivity, σ, of the synthesized composites was measured at room temperature by using the 4-point probe technique, and the results are as shown in Table 2.

Table 2. Conductivity measurements.

Composite	σ, S/m
PBM0	0.1454
PBM1	1.2492
PBM2	1.6049
PBM3	1.5839
PBM4	1.8787
PBM5	2.0320

The samples showed a generally increasing trend of the electrical conductivity as the MWCNT content within the composite was increased. The largest value of σ was observed for the sample with MWCNT wt% loading of 25% with a value of 2.0320 S/m. The good conducting nature of MWCNT results in the improvement the overall electrical conductivity of the composite material [20].

3.3. Electromagnetic Characterization

As implied by the term, the shielding effectiveness (SE) of a material is a suitable constant to gauge the performance of a material to shield against electromagnetic interference. SE, normally expressed in dB, is defined as the ratio between the transmitted power, P_t, and the original incident power, P_0, and is given by SE (dB) $= -10\log(P_t/P_i)$. The shielding effective can then be further expressed as the combined effect of the shielding due to absorption, SE_A, reflection, SE_R, and multiple reflections, SE_M, which results in $SE = SE_A + SE_R + SE_M$. In this study, electromagnetic measurements were performed on the composites by using a two-port network analyzer and expressed in terms of the S-parameters, S_{11}, S_{21}, S_{12}, and S_{21} which represent the reflection coefficient, R, through $R = |E_r/E_i|^2 = |S_{11}|^2 = |S_{22}|^2$, and transmission coefficient, T, through $T = |E_t/E_i|^2 = |S_{21}|^2 = |S_{12}|^2$. The absorption coefficient, A, is thus able to be defined as $A = 1 - R - T$. The value of A at this stage is defined with respect to the initial incident EM energy. After taking into account the reflection at the air-material interface and the negligible effect of multiple reflections on both material interfaces, the intensity of the EM wave propagating within the material can be defined as $1 - R$ which then enables the calculation of the effective absorbance (A_{eff}), where $A_{eff} = (1 - R - T)/(1 - R)$ [21, 22]. Therefore, it is possible to express SE_R and SE_A as $SE_R = -10\log(1 - R)$ and $SE_A = -10\log(1 - A_{eff}) = -10\log(T/(1 - R))$.

The shielding effectiveness of the different synthesized samples are illustrated in Figures 4 and 5. The values of SE_R for all composites show an overall decreasing trend with respect to the increasing frequency of the electromagnetic wave. In contrast, the value of SE_A is seen to increase with each increase in frequency. The biggest values for both shielding effectiveness constants are shown by the sample with 20wt% loading of MWCNT, PBM4, with the SE_R and SE_A values of 5.14 dB at 8.2 GHz

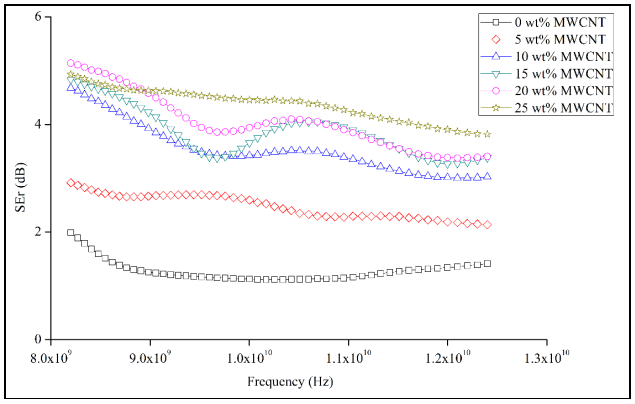

Figure 4. Reflection loss of synthesized composites.

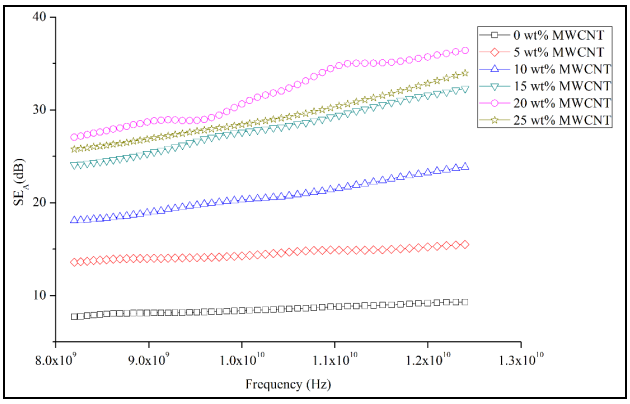

Figure 5. Absorption loss of synthesized composites.

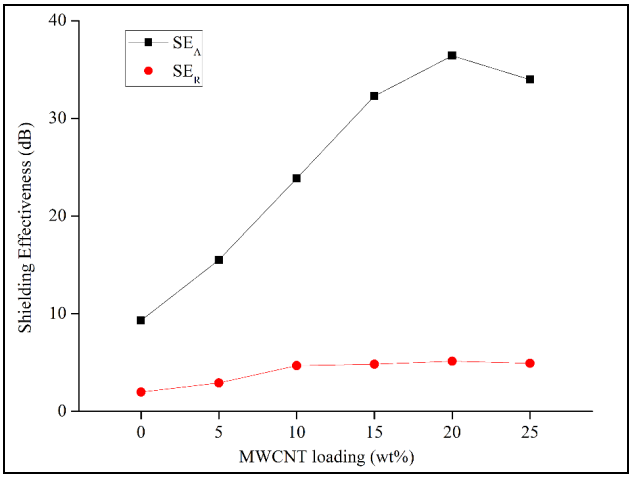

Figure 6. Effect of different MWCNT loading towards the shielding effectiveness.

and 36.41 dB at 12.4 GHz, respectively. The lowest EMI SE values are seen in the composite without any presence of MWCNT. The values of SE_R and SE_A measured for sample PBM0 are 1.11 dB at 10.1 GHz and 7.72 dB at 8.2 GHz, respectively.

The effect on the different MWCNT loadings can be best summarized in Figure 6. The shielding effectiveness shows a similar trend for both parameters where EMI values increase with each increase in the MWCNT content with the exception of the SE_A for sample PBM5 (25wt% MWCNT). The shielding effectiveness due to absorption is lower at all measured frequency than that of sample PBM4 (20wt% MWCNT). With respect to the classical electromagnetic theory, the shielding effectiveness due to absorption can be expressed as [23]:

$$SE_A(\text{dB}) = 20(d/\delta)\log e = 20d(\omega\mu_r\sigma_{ac}/2)^{1/2}\log e \quad (1)$$

where d, δ, ω, μ_r, σ_{ac} are the shield thickness, skin depth, angular frequency, relative magnetic permeability and frequency dependent conductivity ($\sigma_{ac} = \omega\varepsilon_o\varepsilon''$), respectively. Equation (1) shows the dependence of the SE_A on the intrinsic parameters of the material including its conductivity. Based on the equation it was indicated that apart from the permeability, by increasing the conductivity, the shielding performance would be improved. However, it is also important to note that impedance of materials possessing very high conductivities tends to be relatively small compared to that of air, causing a relative mismatch which results in more electromagnetic wave to be reflected back [14]. This explains the slight drop of SE_A and the simultaneous increase of the SE_R after increasing the MWCNT

loading to 25wt% from 20wt%.

As the composite samples consist of materials either magnetic or dielectric in nature, it is thus useful to determine the contribution of each constituent of the composite material in terms of another electromagnetic parameter called the loss angle tangent, $\tan\delta$ [24]. The magnetic loss angle tangent is defined as $\tan\delta_\mu = \mu''/\mu'$ and the dielectric loss tangent as $\tan\delta_\varepsilon = \varepsilon''/\varepsilon'$. As the loss mechanism in a material is closely related to both imaginary components of relative permeability (μ'') and permittivity (ε''), a big value of loss angle tangent would imply a better electromagnetic absorption performance. The variations of the magnetic and dielectric tangential losses in each MWCNT loading with respect to frequency are shown in Figures 7 and 8, respectively.

The initial addition of MWCNT resulted in a slight drop in the magnetic loss as observed when the MWCNT content was increased from 0 (PBM0) to 5 (PBM1) wt%. However, this trend changed with further increase in the MWCNT loading. Samples PBM2, PBM3, PBM4 and PBM5 showed an upward trend with the magnitude of the magnetic tangential loss increasing for each sample. The biggest value of magnetic loss angle is 6.65, observed in sample PBM5 at 8.2 GHz which suggests a value of ε'' six times larger than the value of ε'.

The decreasing magnetic ferrite component alongside the simultaneous increase in the non-magnetic MWCNT and PANI points towards a decrease in the magnetic tangential loss. However, the opposite happens which can again be attributed to the increasing conductive nature of the composite as the MWCNT loading increases. A conductive material subjected to an alternating magnetic field would produce an induced current that was able to dissipate energy within the material [25, 26]. The induced current is known as the eddy current loss and is one of the magnetic loss mechanisms, other than the hysteresis and residual loss.

In Figure 7, it can be seen that there exist fluctuations in the value dielectric tangential loss when being taken as a function of either the MWCNT loading or the frequency especially between samples with 5wt%, 10wt%, and 15wt% MWCNT loading. However, the magnitude of the losses is still significantly higher than that of the sample with 0wt% MWCNT. A further 5wt%-step increase in the MWCNT content results in a drastic increase in the magnitude of dielectric loss angle tangent. Sample PBM4 shows a 4-fold increase in losses compared to the previous samples with values of dielectric loss angle tangent ranging between 3 to 5, along the frequency range. It is also important to note that there exists a resonance peak at 9.36 GHz with the magnitude of loss angle reaching the value of 24.91. With the exception for loss angle tangent values recorded at frequencies lower than 9 GHz, the magnitudes of loss angle tangent for the sample with 20wt% MWCNT loading are larger than that of the other synthesized samples for the rest of the frequency range. Sample PBM5 with 25wt% MWCNT loading shows a slight decrease in the tangential loss at frequencies between 9 GHz and 12.4 GHz compared to sample PBM4.

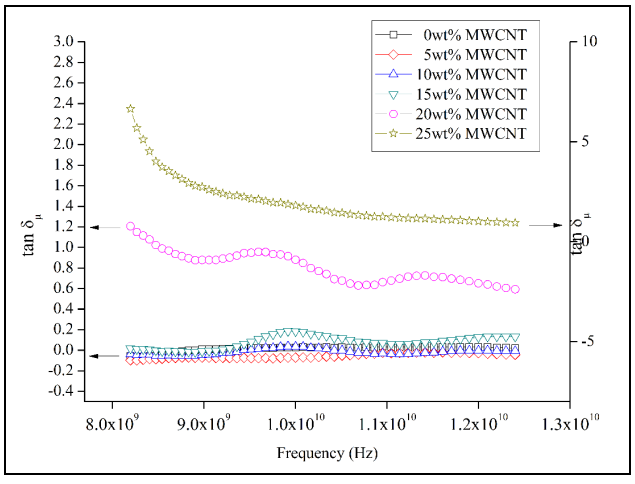

Figure 7. Magnetic loss angle tangent variation with different MWCNT loadings with respect to frequency.

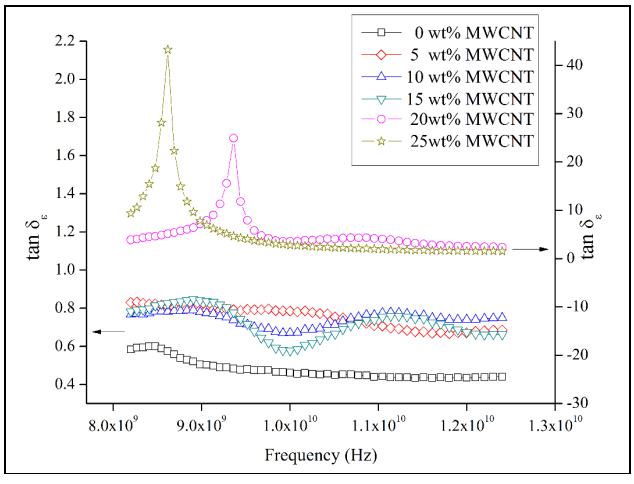

Figure 8. Dielectric loss angle tangent variation with different MWCNT loadings with respect to frequency.

However, the existence of a resonance peak at 8.61 GHz results in the largest value of dielectric loss angle tangent recorded with the value reaching 43.24. This can be attributed to the significantly large value of the imaginary component of permittivity, ε'', compared to its real counterpart, ε'.

As the electromagnetic energy loss due to absorption is the combined effects of both the dielectric and magnetic components of the synthesized composites, the algebraic sum of both tangential losses is equal to the gross loss angle tangent [27]. The significantly big difference between the magnitude of the dielectric and magnitude loss angle tangent observed for all synthesized samples suggests that the main mechanism of absorption is the dielectric losses. The introduction of MWCNT leads to the overall increase in the electrical conductance of the material, which, combined with the conductive nature of PANI, will lead to the enhancement of loss mechanisms such as conductance and dielectric losses [14]. However, the drop in the SE_A values after the MWCNT loading reaches 25wt% suggests that there exists a certain threshold for the MWCNT loading which will help to enhance the absorption capability of the shielding material before the electromagnetic energy is reflected back. This involves the complex interplay between the ratio between the constituents of the composite and the intrinsic properties (magnetic and dielectric) of said constituents.

4. CONCLUSION

The composite material consisting of $BaFe_{12}O_{19}$, MWCNT and PANI is successfully synthesized through a simple *in-situ* polymerization technique. XRD analysis reveals that the increasing addition of MWCNT in the composite will result in the slight decrease in the relative intensity due to the reduced amount of crystalline ferrite in the composite. FESEM micrographs reveal that the PANI particles form on the $BaFe_{12}O_{19}$ and MWCNT surfaces and differ from their usual tubular form. Electromagnetic measurement reveals promising values EMI shielding effectiveness especially through absorption. The increase in the MWCNT results in the enhanced performance of the shielding effectiveness through absorption. However, there exists a threshold for the MWCNT incorporation before the electromagnetic waves are reflected back resulting in decreased absorbing performance.

ACKNOWLEDGMENT

The author would like to express their gratitude toward Universiti Teknologi Petronas (UTP) and Universiti Malaysia Perlis (UniMAP) for providing the facilities and technical support leading to the completion of this research work.

REFERENCES

1. Tong, X. C., *Advanced Materials and Design for Electromagnetic Interference Shielding*, Taylor & Francis, 2008.
2. Hibst, H., "Hexagonal ferrites from melts and aqueous solutions, magnetic recording materials," *Angewandte Chemie International Edition in English*, Vol. 21, 270–282, 1982.
3. Lotgering, F. K., P. R. Locher, and R. P. van Stapele, "Anisotropy of hexagonal ferrites with M, W and Y structures containing Fe3+ and Fe2+ as magnetic ions," *Journal of Physics and Chemistry of Solids*, Vol. 41, 481–487, 1980.
4. Albanese, G., A. Deriu, and S. Rinaldi, "Sublattice magnetization and anisotropy properties of $Ba_3Co_2Fe_{24}O_{41}$ hexagonal ferrite," *Journal of Physics C: Solid State Physics*, Vol. 9, 1313, 1976.
5. Xu, P., X. Han, and M. Wang, "Synthesis and magnetic properties of $BaFe_{12}O_{19}$ hexaferrite nanoparticles by a reverse microemulsion technique," *The Journal of Physical Chemistry C*, Vol. 111, 5866–5870, 2007.
6. Liu, J., P. Liu, X. Zhang, D. Pan, P. Zhang, and M. Zhang, "Synthesis and properties of single domain sphere-shaped barium hexa-ferrite nano powders via an ultrasonic-assisted co-precipitation route," *Ultrasonics Sonochemistry*, Vol. 23, 46–52, March 2015.
7. Saini, P., V. Choudhary, B. P. Singh, R. B. Mathur, and S. K. Dhawan, "Polyaniline-MWCNT nanocomposites for microwave absorption and EMI shielding," *Materials Chemistry and Physics*, Vol. 113, 919–926, 2009.

8. Duan, Y., L. Shunhua, and G. Hongtao, "Investigation of electrical conductivity and electromagnetic shielding effectiveness of polyaniline composite," *Science and Technology of Advanced Materials*, Vol. 6, 513–518, 2005.
9. Singh, K., A. Ohlan, V. H. Pham, B. R, S. Varshney, J. Jang, S. H. Hur, W. M. Choi, M. Kumar, S. K. Dhawan, B.-S. Kong, and J. S. Chung, "Nanostructured graphene/Fe_3O_4 incorporated polyaniline as a high performance shield against electromagnetic pollution," *Nanoscale*, Vol. 5, 2411–2420, 2013.
10. Sharma, B. K., N. Khare, R. Sharma, S. K. Dhawan, V. D. Vankar, and H. C. Gupta, "Dielectric behavior of polyaniline–CNTs composite in microwave region," *Composites Science and Technology*, Vol. 69, 1932–1935, 2009.
11. Han, M. and L. Deng, *High Frequency Properties of Carbon Nanotubes and Their Electromagnetic Wave Absorption Properties*, J. M. Marulanda, Ed., Carbon Nanotubes Applications on Electron Devices, InTech, 2011.
12. Qin, F. and C. Brosseau, "A review and analysis of microwave absorption in polymer composites filled with carbonaceous particles," *Journal of Applied Physics*, Vol. 111, 061301, 2012.
13. Pullar, R. C., "Hexagonal ferrites: A review of the synthesis, properties and applications of hexaferrite ceramics," *Progress in Materials Science*, Vol. 57, 1191–1334, 2012.
14. Huo, J., L. Wang, and H. Yu, "Polymeric nanocomposites for electromagnetic wave absorption," *Journal of Materials Science*, Vol. 44, 3917–3927, 2009.
15. Wang, Y., "Research progress on nanostructured radar absorbing materials," *Energy and Power Engineering*, Vol. 03, 580–584, 2011.
16. Tadjarodi, A., H. Kerdari, and M. Imani, "$Ba_{0.69}Sr_{0.17}Cd_{0.07}Zn_{0.07}Fe_{12}O_{19}$ nanostrucutres/conducting polyaniline nanocomposites; synthesis, characterization and microwave absorption performance," *Journal of Alloys and Compounds*, Vol. 554, 284–292, 2013.
17. Fan, Z., G. Luo, Z. Zhang, L. Zhou, and F. Wei, "Electromagnetic and microwave absorbing properties of multi-walled carbon nanotubes/polymer composites," *Materials Science and Engineering: B*, Vol. 132, 85–89, 2006.
18. Dhawan, S. K., K. Singh, A. K. Bakhshi, and A. Ohlan, "Conducting polymer embedded with nanoferrite and titanium dioxide nanoparticles for microwave absorption," *Synthetic Metals*, Vol. 159, 2259–2262, 2009.
19. Goldman, A., *Modern Ferrite Technology*, Springer Science & Business Media, 2006.
20. Bandaru, P. R., "Electrical properties and applications of carbon nanotube structures," *Journal of Nanoscience and Nanotechnology*, Vol. 7, 1239–1267, 2007.
21. Phan, C. H., M. Mariatti, and Y. H. Koh, "Electromagnetic interference shielding performance of epoxy composites filled with multiwalled carbon nanotubes/manganese zinc ferrite hybrid fillers," *Journal of Magnetism and Magnetic Materials*, Vol. 401, 472–478, 2016.
22. Wang, Z., G. Wei, and G. L. Zhao, "Enhanced electromagnetic wave shielding effectiveness of Fe doped carbon nanotubes/epoxy composites," *Applied Physics Letters*, Vol. 103, 183109, 2013.
23. Verma, V., J. Kapil, and N. Singh, "Structural, magnetic properties of soft and hard ferrites and their emi shielding application in X-band frequency range," *International Journal of Engineering Research & Technology (IJERT)*, 557–560, 2014.
24. Malek, M. F. B. A., E. M. Cheng, O. Nadiah, H. Nornikman, M. Ahmed, M. Z. A. Abdul Aziz, A. R. Othman, P. J. Soh, A. A. A.-H. Azremi, A. Hasnain, and M. N. Taib, "Rubber tire dust-rice husk pyramidal microwave absorber," *Progress In Electromagnetics Research*, Vol. 117, 449–477, 2011.
25. Stoll, R. L., *The Analysis of Eddy Currents*, Oxford University Press, 1974.
26. Pry, R. H. and C. P. Bean, "Calculation of the energy loss in magnetic sheet materials using a domain model," *Journal of Applied Physics*, Vol. 29, 532–533, 1958.
27. Li, Y., Y. Huang, S. Qi, L. Niu, Y. Zhang, and Y. Wu, "Preparation, magnetic and electromagnetic properties of polyaniline/strontium ferrite/multiwalled carbon nanotubes composite," *Applied Surface Science*, Vol. 258, 3659–3666, 2012.